Available online at www.sciencedirect.com
ScienceDirect
Computers and Structures 86 (2008) 1369–1384
Computers & Structures
www.elsevier.com/locate/compstruc

Design sensitivity analysis of nonlinear structures subjected to thermal loads

Evandro Parente Jr. [a,*], João Batista Marques de Sousa Jr. [b]

[a] Department of Structural Engineering, Federal University of Ceará, Campus do Pici, Bloco 710, 60455-760, Fortaleza, Ceará, Brazil
[b] Department of Civil Engineering, Federal University of Ouro Preto, Brazil

Received 1 August 2006; accepted 29 August 2007
Available online 1 November 2007

Abstract

This work presents a simple and efficient methodology for sensitivity analysis of geometrically nonlinear structures subjected to thermo-mechanical loading in regular and critical states. Using the effective strain approach, the path-following methods and the algorithms for critical point computation developed originally for finite element analysis of mechanically loaded structures are modified to include the thermal effects. The general expressions for sensitivity computation of displacements, stresses and nonlinear critical loads are obtained through the differentiation of the finite element equations. The practical implementation of the sensitivity analysis in a finite element code employing the Analytical, Semi-Analytical and Refined Semi-Analytical approaches is discussed in detail. Finally, a set of numerical examples is used to validate the proposed methodology.

Keywords: Design sensitivity analysis; Structural optimization; Thermal loads; Nonlinear structures

1. Introduction

Several structures and mechanical components are subjected simultaneously to mechanical and thermal loading. It is well known that a temperature increase causes displacements and strains in structures whose expansion is not constrained, and that the so-called thermal stresses are generated when the free thermal expansion is restrained by supports or friction. Practical experience has shown that a temperature increase can create enough compressive stresses to cause buckling of slender structures. Therefore, thermal buckling is an important issue in the design of heated structures, like columns, pipelines, plates and shells.

The design optimization of structures including thermal buckling constraints has attracted much attention in the recent years, see [1] and references therein. However, most of these works are based on small displacement analysis and linearized buckling procedures, which limits the applicability of the proposed optimization formulations. As a matter of fact, the optimization of slender structures can lead to severe instability problems, including imperfection sensitivity and modal interaction [2]. It was observed that stability problems tend to occur when the optimization is based on the assumption of linear structural behavior [3].

In order to avoid these problems, the geometrically nonlinear effects should be considered in the structural analysis and the optimum design formulation should include an appropriate set of stability constraints [4]. It is also important to include the effects of load and geometry imperfections in the optimization model [5,6]. Generally, the presence of initial imperfections eliminates the bifurcation points, yielding either limit points for asymmetrical and unstable symmetric bifurcations or stable paths without critical points for stable-symmetric bifurcations [7]. In the latter case, large deflections can arise and appropriate displacement constraints should be included in the optimization model.

It should be noted that a uniform temperature field in a structure without geometric imperfections will generally

* Corresponding author. Tel.: +55 85 3366 9607.
E-mail address: evandro@ufc.br (E. Parente Jr.).

0045-7949/$ - see front matter © 2007 Elsevier Ltd. All rights reserved.
doi:10.1016/j.compstruc.2007.08.002

preserve the critical states typical of perfect structures. On the other hand, a nonuniform field with a temperature gradient in the transverse direction of beams, plates and shells generates initial deflections which can eliminate the critical states even for perfect structures. Therefore, the effects of thermally induced bending should also be considered either alone or combined with geometric imperfections.

In this work, the thermal effects are included in the finite element formulation through the effective strain concept, leading to a simple and generic procedure for computation of the internal force vector and stiffness matrix of different finite elements [8]. The analysis procedure presented here can handle structures under pure mechanical loading, pure thermal loading and combined thermo-mechanical loading.

The determination of the load-carrying capacity of structures subjected to mechanical loads and temperature variations require the use of robust methods to trace the nonlinear equilibrium paths and to perform the critical point computation. These methods will be discussed here with focus on the relevant aspects to the sensitivity computation. Both perfect and imperfect structures will be considered.

The most efficient algorithms for structural optimization, as the Sequential Quadratic Programming (SQP) method, require the gradients of the objective and constraint functions to compute the search direction at each step of the optimization process [9,10]. Errors in computation of these gradients can degrade the performance of the optimization algorithm and lead to severe convergence problems. The gradients of the constraint functions depend on the derivatives (sensitivities) of structural responses, as displacements, stresses, and critical loads, with respect to the design variables. Therefore, the use of efficient and accurate procedures to perform sensitivity analysis is paramount to the success of the structural optimization process. In addition, sensitivity analysis has also other important applications, as parameter identification [11] and structural reliability analysis [12].

It is important to note that this paper is concerned only with the sensitivity of the structural responses, but methods to compute the sensitivity of the temperature field are readily available [13,14]. Therefore, in this work it is assumed that the temperature field and its sensitivity were previously computed and given to the structural analysis program as input data.

The general expressions for computation of design sensitivities in regular and critical states are obtained through the direct differentiation of the finite element equations. This approach leads to expressions required to the computation of displacements, stresses and nonlinear critical (limit and bifurcation) loads for both size and shape variables. The adjoint approach will also be applied to the computation of sensitivity of the nonlinear critical loads [15,16]. It results in a more efficient procedure than the direct one, but it will be shown that it can be used only for symmetric bifurcation points.

According to the dependence of the temperature field on the design variables, the sensitivities can be classified as coupled or uncoupled [1]. Most of the previous works are focused on the uncoupled case [15,6]. On the other hand, this work focuses on the coupled case and the dependence of the temperature field on the design variables is accounted for. It will be shown that the modifications in the sensitivity expressions required to consider the temperature variations are very similar to those performed in the path-following methods and in the procedures for critical point computation. The expressions for uncoupled sensitivities are easily obtained from the general expressions eliminating the terms related to the sensitivity of the temperature field.

The sensitivity formulation presented in this work can be applied to structures subjected to pure mechanical loading, pure thermal loading and combined thermo-mechanical loading. The procedure is independent of the element formulation and handles both perfect and imperfect structures in regular and critical states.

The expressions for sensitivity computation depend on the derivatives of the element vectors and matrices with respect to the design variables. These derivatives are computed here using the Analytical, Semi-Analytical and Refined Semi-Analytical Methods [17–20]. Numerical examples are presented to validate the proposed methodology and to assess the accuracy of the conventional and refined semi-analytical approaches for shape variables.

2. Finite element analysis

The finite element analysis of structures subjected to thermal loading will be briefly discussed here. The objective is to present some features that are important to the derivation of the expressions used in the sensitivity analysis, which will be effectively carried out in Section 3. More details of FE procedures used to trace the complete nonlinear equilibrium paths of structures subject to thermal loading, including algorithms to trace the secondary (post-buckling) paths are presented in [8].

In order to include the thermal effects in the analysis of structures it is necessary to modify the relations between stresses ($\boldsymbol{\sigma}$) and strains ($\boldsymbol{\varepsilon}$) to consider the expansion due to temperature changes. For linear elastic materials, the stress–strain–temperature relation can be written as

$$\boldsymbol{\sigma} = \mathbf{C}(\boldsymbol{\varepsilon} - \boldsymbol{\varepsilon}_{\mathrm{th}}), \tag{1}$$

where $\mathbf{C}$ is the temperature-dependent elastic constitutive matrix and $\boldsymbol{\varepsilon}_{\mathrm{th}}$ are thermal strains of a solid whose expansion is not constrained.

The thermal strains of a 3D isotropic solid can be computed from

$$\boldsymbol{\varepsilon}_{\mathrm{th}} = \boldsymbol{\alpha}\Delta T \quad \text{with } \boldsymbol{\alpha}^{\mathrm{t}} = [\,\alpha \quad \alpha \quad \alpha \quad 0 \quad 0 \quad 0\,], \tag{2}$$

where α is the thermal expansion coefficient and ΔT is the temperature variation. Similar expressions arise for plane stress, plane strain, and axisymmetric solid models.

For structural elements such as beams, plates and shells, the problem is more complex, since a nonuniform temperature distribution along the cross section leads to bending as well as membrane strains. Therefore, for a beam element based on the Euler theory, one can write

$$\boldsymbol{\varepsilon}_{\mathrm{ef}} = \boldsymbol{\varepsilon} - \boldsymbol{\varepsilon}_{\mathrm{th}} = \begin{bmatrix} \varepsilon \\ \kappa \end{bmatrix} - \begin{bmatrix} \varepsilon_{\mathrm{th}} \\ \kappa_{\mathrm{th}} \end{bmatrix}, \tag{3}$$

where ε is the axial strain and κ is the curvature. Considering a linear temperature distribution along height (h) of the cross section of a plane beam, the generalized thermal strains are given by

$$\begin{bmatrix} \varepsilon_{\mathrm{th}} \\ \kappa_{\mathrm{th}} \end{bmatrix} = \begin{bmatrix} \alpha \Delta T_{\mathrm{c}} \\ \alpha \frac{\Delta T_{\mathrm{top}} - \Delta T_{\mathrm{bot}}}{h} \end{bmatrix}, \tag{4}$$

where ΔT_{c}, ΔT_{top} and ΔT_{bot} are temperature changes at the centroid, top and bottom of the cross section, respectively. Similar expressions can be written for plates and shells. It is important to note that a temperature gradient in the cross section may induce initial deflections which combined with geometric imperfections may eliminate the bifurcation points, generating limit points and large displacements.

Eq. (1) shows that for thermally loaded structures the stresses are not linked directly to the total strain, as in the case of mechanically loaded structures, but are caused by an 'effective strain'

$$\boldsymbol{\sigma} = \mathbf{C}\boldsymbol{\varepsilon}_{\mathrm{ef}}, \;\Rightarrow\; \boldsymbol{\varepsilon}_{\mathrm{ef}} = \boldsymbol{\varepsilon} - \boldsymbol{\varepsilon}_{\mathrm{th}}. \tag{5}$$

Using the Virtual Work Principle, the internal force vector ($\mathbf{g}$) of a given finite element is given by

$$\delta W_{\mathrm{int}} = \delta \mathbf{u}_{\mathrm{v}}^{\mathrm{t}} \mathbf{g} = \int_V \delta \boldsymbol{\varepsilon}_{\mathrm{v}}^{\mathrm{t}} \boldsymbol{\sigma} \, \mathrm{d}V, \tag{6}$$

where $\delta\boldsymbol{\varepsilon}_{\mathrm{v}}$ is virtual strain field within the element and $\delta\mathbf{u}_{\mathrm{v}}$ is the virtual displacement of the element nodes. Therefore, the internal force vector can be computed from

$$\mathbf{g} = \int_V \overline{\mathbf{B}}^{\mathrm{t}} \boldsymbol{\sigma} \, \mathrm{d}V, \quad \text{since } \delta\boldsymbol{\varepsilon}_{\mathrm{v}} = \overline{\mathbf{B}} \delta \mathbf{u}_{\mathrm{v}}. \tag{7}$$

For large displacement analysis, the incremental strain–displacement matrix ($\overline{\mathbf{B}}$) depends on the nodal displacements.

2.1. Path-following methods

The aim of the path-following methods is to trace the equilibrium path of a given structure, providing valuable information about its behavior and load-carrying capacity. Considering a structure subjected to a set of displacement independent loads, as well as to temperature changes, the global equilibrium equations of a finite element model can be written as

$$\mathbf{r}(\mathbf{u}, \lambda) = \mathbf{g}(\mathbf{u}, \lambda) - (\lambda \mathbf{f} + \mathbf{f}_{\mathrm{c}}), \tag{8}$$

where $\mathbf{r}$ is the out-of-balance force vector, $\mathbf{f}_{\mathrm{c}}$ is the vector of constant loads, $\mathbf{f}$ is the reference load vector for proportional loads, and λ is the load factor. The equilibrium path is the set of points $(\mathbf{u}, \lambda)$ which satisfies Eq. (8). An example of such curve is shown in Fig. 1.

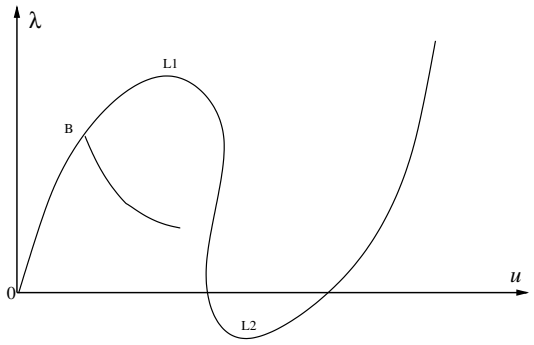

Fig. 1. Complex equilibrium path.

The consideration of $\mathbf{f}_{\mathrm{c}}$ in Eq. (8) is important to some applications where it is necessary to apply the dead load (self-weight) first and then to increase the live load or the temperature. It should be noted that the load factor controls the application of the proportional loads as is the standard procedure in nonlinear finite element analysis. However, here λ also controls the applied temperature by using

$$T = T_{\mathrm{ref}} + \lambda(\overline{T} - T_{\mathrm{ref}}), \tag{9}$$

where T_{ref} is the reference temperature and $\overline{T}$ is the temperature corresponding to the $\lambda = 1$. Therefore, the temperature change at a given step is given by

$$\Delta T = T - T_{\mathrm{ref}} = \lambda(\overline{T} - T_{\mathrm{ref}}) = \lambda \Delta \overline{T}. \tag{10}$$

This formulation allows the analysis of structures subjected to pure mechanical loading ($\Delta\overline{T} = 0$), pure thermal loading ($\mathbf{f} = \mathbf{0}$) and combined thermo-mechanical loading ($\Delta\overline{T} \neq 0$ and $\mathbf{f} \neq \mathbf{0}$).

The temperatures T_{ref} and $\overline{T}$ can be associated with the elements or nodes of the finite element mesh. In the latter case it is necessary to use an interpolation scheme in order to obtain the temperature within the element. Moreover, for beam, plates, and shells it is possible to define the temperatures of the inferior and superior surfaces in order to model the thermally induced bending.

It is important to note that the reference temperature is generally constant for the entire mesh while the spatial distribution of $\overline{T}$ may be computed by a steady-state thermal analysis [21,22]. It is assumed here that this thermal analysis was successfully carried out previously and that the computed temperatures are given to the structural analysis program as input data.

The system of nonlinear equations described by Eq. (8) has $N + 1$ variables, but only N equations, where N is the number of degrees of freedom (dofs) of the FE model. The principle of the Load Control Method is to eliminate one variable prescribing the load factor at the beginning of each step and keeping it fixed during the iterative process. Therefore, the linearization of Eq. (8) yields

$$\mathbf{r}_{i+1} = \mathbf{r}_i + \mathbf{r}_{,\mathbf{u}}\delta\mathbf{u} = \mathbf{r}_i + \mathbf{K}\,\delta\mathbf{u}, \tag{11}$$

where $\mathbf{K}$ is the tangent stiffness matrix ($\mathbf{K} = \mathbf{r}_{,\mathbf{u}}$) and i is the iteration number. The iterative correction $\delta\mathbf{u}$ can be computed setting $\mathbf{r}_{i+1} = \mathbf{0}$, which leads to the linear system

$$\mathbf{K}\,\delta\mathbf{u} = -\mathbf{r}_i \Rightarrow \mathbf{K}\,\delta\mathbf{u} = \mathbf{f}_c + \lambda\mathbf{f} - \mathbf{g}_i. \tag{12}$$

After $\delta\mathbf{u}$ computation, the nodal displacements are updated using

$$\mathbf{u}_{i+1} = \mathbf{u}_i + \delta\mathbf{u}. \tag{13}$$

The iterations continue until the norm of the residual vector becomes smaller than a prescribed tolerance.

Since pressure loads are not considered here, $\mathbf{f}$ does not depend on $\mathbf{u}$. Thus, the stiffness matrix can be computed from the linearization of the internal force vector leading to

$$\mathrm{d}\mathbf{g} = \mathbf{K}\,\mathrm{d}\mathbf{u} = \int_V \mathrm{d}\overline{\mathbf{B}}^{\mathrm{t}}\boldsymbol{\sigma}\,\mathrm{d}V + \int_V \overline{\mathbf{B}}^{\mathrm{t}}\mathrm{d}\boldsymbol{\sigma}\,\mathrm{d}V = \mathbf{K}_e\mathrm{d}\mathbf{u} + \mathbf{K}_g\mathrm{d}\mathbf{u}, \tag{14}$$

which is exactly the same expression obtained for the standard case of mechanical loading. As a consequence, the consideration of temperature variations does not require any modification in the computer implementation of the Load Control Method used for pure mechanical loads. The thermal effects are indirectly included in the iterative process due to the dependence of the internal force vector ($\mathbf{g}$) and the geometric stiffness matrix ($\mathbf{K}_g$) on the element stresses [8].

The Load Control Method is widely used for nonlinear analysis of structures, but it cannot trace the equilibrium path beyond limit points. In fact, in the case of Fig. 1, the Load Control Method would either fail to converge after point L1 or to snap directly to the stable branch, providing incomplete or misleading information about the stability of the structure. To overcome this problem, it is necessary to use more complex path-following techniques, such as the Displacement Control Method [23] or the Arc-Length Method [24–26].

The system of nonlinear equations given by Eq. (8) has $N+1$ variables, but only N equations. To overcome this difficulty and keep λ as a variable, which is required in order to overcome limit points, it is necessary to add a constraint equation $f(\mathbf{u},\lambda)$, leading to

$$\begin{bmatrix}\mathbf{r}(\mathbf{u},\lambda)\\ f(\mathbf{u},\lambda)\end{bmatrix} = \mathbf{0}, \tag{15}$$

where the constraint equation f is different for each Constrained Newton–Raphson Method [26,5]. As a practical example, the constraint for the Arc-Length Method is given by

$$f = \Delta\mathbf{u}^{\mathrm{t}}\Delta\mathbf{u} + \psi^2\Delta\lambda^2 - \Delta l^2 = 0, \tag{16}$$

where $\Delta\mathbf{u}$ and $\Delta\lambda$ are incremental changes, Δl is the prescribed arc-length and ψ is a scaling parameter.

The expression required to compute the iterative corrections $\delta\mathbf{u}$ and $\delta\lambda$ can be obtained by the linearization of Eq. (15), yielding

$$\begin{bmatrix}\mathbf{K} & \mathbf{r}_{,\lambda}\\ f^{\mathrm{t}}_{,\mathbf{u}} & f_{,\lambda}\end{bmatrix}\begin{bmatrix}\delta\mathbf{u}\\ \delta\lambda\end{bmatrix} = -\begin{bmatrix}\mathbf{r}\\ f\end{bmatrix}. \tag{17}$$

Instead of solving directly the system above with $N+1$ equations and a nonsymmetric matrix, it is more efficient to use a partitioning scheme [23]. Thus, the first equation is written as

$$\mathbf{K}\,\delta\mathbf{u} = \delta\lambda\bar{\mathbf{f}} - \mathbf{r}, \tag{18}$$

where

$$\bar{\mathbf{f}} = -\mathbf{r}_{,\lambda} = \mathbf{f} - \mathbf{g}_{,\lambda}. \tag{19}$$

Now, the iterative displacements can be computed from

$$\delta\mathbf{u} = \delta\lambda\,\delta\bar{\mathbf{u}} + \delta\hat{\mathbf{u}} \quad \text{with} \quad \begin{cases}\mathbf{K}\,\delta\bar{\mathbf{u}} = \bar{\mathbf{f}},\\ \mathbf{K}\,\delta\hat{\mathbf{u}} = -\mathbf{r}.\end{cases} \tag{20}$$

It is important to note that the approach used here will also be applied in the algorithms for critical point computation and in the derivation of the expressions for sensitivity analysis of bifurcation points. Finally, substituting (20) in the second row of (17) the iterative change of the load factor is given by

$$\delta\lambda = -\frac{f^{\mathrm{t}}_{,\mathbf{u}}\delta\hat{\mathbf{u}} + f}{f^{\mathrm{t}}_{,\mathbf{u}}\delta\bar{\mathbf{u}} + f_{,\lambda}}. \tag{21}$$

It should be noted that for structures subjected to pure mechanical loading, the internal forces ($\mathbf{g}$) do not depend on the load factor. As a consequence $\mathbf{g}_{,\lambda} = \mathbf{0}$ and $\bar{\mathbf{f}} = \mathbf{f}$. Thus, the previous equations reduce to the standard case discussed in the literature [26]. On the other hand, to trace the equilibrium paths of structures with thermal loading it is necessary to compute the vector $\mathbf{g}_{,\lambda}$. The differentiation of Eq. (7) with respect to λ yields

$$\mathbf{g}_{,\lambda} = \int_V \overline{\mathbf{B}}^{\mathrm{t}}\boldsymbol{\sigma}_{,\lambda}\,\mathrm{d}V \quad \text{with } \boldsymbol{\sigma}_{,\lambda} = \left[\frac{\partial\boldsymbol{\sigma}}{\partial p_i}\frac{\partial p_i}{\partial T} - \mathbf{C}\left(\boldsymbol{\alpha} + \frac{\partial\boldsymbol{\alpha}}{\partial T}\Delta T\right)\right]\Delta\overline{T}, \tag{22}$$

where p_i represents a material parameter, as the Young modulus or the Poisson ratio, and the summation convention for repeated indices was used.

The vector $\mathbf{g}_{,\lambda}$ can be readily computed using Eq. (22). However, this requires the implementation and testing of a new function for each finite element type, which is a challenging task for a large FE program. On the other hand, using the standard forward difference scheme, $\mathbf{g}_{,\lambda}$ can be computed from

$$\mathbf{g}_{,\lambda} = \frac{\mathbf{g}(\mathbf{u},\lambda+\Delta\lambda) - \mathbf{g}(\mathbf{u},\lambda)}{\Delta\lambda}, \tag{23}$$

where $\Delta\lambda$ is the perturbation size (typically between 10^{-3} and 10^{-7}). The main advantage of this approach is that it

does not depend on the element type. Therefore, it can be implemented only once at the global level of the finite element program and used with any finite element available in the analysis program. Eq. (23) is efficient since $\mathbf{g}(\mathbf{u},\lambda)$ was already computed for the evaluation of the residual forces ($\mathbf{r}$). Moreover, for the important case of linear elastic materials with temperature-independent properties, Eq. (23) leads to exact results since in this case $\mathbf{g}$ depends linearly on λ.

2.2. Stability analysis

The analysis of a given structure is not complete without the determination of its load carrying capacity, which requires the computation of its critical points. A limit point arises when the equilibrium path reaches a local extremum, as the points L1 (maximum) and L2 (minimum), while a bifurcation occurs when different equilibrium paths cross at a certain point, as the point B in Fig. 1.

A point $(\mathbf{u},\lambda)$ of the load–displacement curve is a critical point when the stiffness matrix of the FE model is singular. Thus, a critical point can be detected using the zero eigenvalue condition

$$\mathbf{K}(\mathbf{u},\lambda)\boldsymbol{\phi} = \mathbf{0} \quad \text{with } \|\boldsymbol{\phi}\| = 1, \tag{24}$$

where $\boldsymbol{\phi}$ is the associated eigenvector, which represents the buckling mode of the structure.

Once detected a critical point, it is necessary to determine whether it is a limit or a bifurcation point. To perform this task, it is convenient to describe the load–displacement curve using a single parameter (s) that never decreases during the loading process, like the total arc-length. Using the parametric form, the equilibrium equation can be written as

$$\mathbf{r}(\mathbf{u}(s),\lambda(s)) = \mathbf{0}, \tag{25}$$

and its differentiation w.r.t. the curve parameter yields

$$\dot{\mathbf{r}} = \mathbf{r}_{,\mathbf{u}}\dot{\mathbf{u}} + \mathbf{r}_{,\lambda}\dot{\lambda} = \mathbf{K}\dot{\mathbf{u}} + \mathbf{r}_{,\lambda}\dot{\lambda} = \mathbf{0}, \tag{26}$$

where $\dot{}$ indicates differentiation with respect to s. Using condition (24) and the symmetry of the stiffness matrix, it can be shown that $\boldsymbol{\phi}^{\mathrm{t}}\mathbf{K} = \mathbf{0}$ at a critical point. Therefore, the multiplication of Eq. (26) by $\boldsymbol{\phi}^{\mathrm{t}}$ leads to

$$(\boldsymbol{\phi}^{\mathrm{t}}\bar{\mathbf{f}})\dot{\lambda} = 0, \tag{27}$$

where $\bar{\mathbf{f}} = -\mathbf{r}_{,\lambda}$. As pointed out early, a limit point is characterized by the fact that the load–displacement curve reaches an extremum value, so the condition $\dot{\lambda} = 0$ must hold for these points. Therefore, the following criterion can be used to classify the critical points:

$$\begin{cases} \boldsymbol{\phi}^{\mathrm{t}}\bar{\mathbf{f}} \neq 0 \Rightarrow \text{limit point}, \\ \boldsymbol{\phi}^{\mathrm{t}}\bar{\mathbf{f}} = 0 \Rightarrow \text{bifurcation point}. \end{cases} \tag{28}$$

It should be emphasized that this classification is of great practical importance to the sensitivity analysis, since the computation of the sensitivity of limit points is much more simple and efficient than for bifurcation points, as will be discussed later.

There are different types of bifurcation points and to classify these points it is necessary to use higher-order terms. The differentiation of Eq. (26) yields

$$\mathbf{K}\ddot{\mathbf{u}} + \mathbf{r}_{,\lambda}\ddot{\lambda} = -(\mathbf{K}_{,\mathbf{u}}\dot{\mathbf{u}}\dot{\mathbf{u}} + 2\mathbf{K}_{,\lambda}\dot{\mathbf{u}}\dot{\lambda} + \mathbf{r}_{,\lambda\lambda}\dot{\lambda}^2). \tag{29}$$

Moreover, the tangent to the equilibrium path at a bifurcation point [27] can be written as

$$\begin{aligned} \dot{\mathbf{u}} &= \xi_0\bar{\mathbf{u}} + \xi_1\boldsymbol{\phi}, \\ \dot{\lambda} &= \xi_0 \end{aligned} \tag{30}$$

with

$$\mathbf{K}\bar{\mathbf{u}} + \mathbf{r}_{,\lambda} = \mathbf{0}, \quad \|\bar{\mathbf{u}}\| = 1 \quad \text{and} \quad \boldsymbol{\phi}^{\mathrm{t}}\bar{\mathbf{u}} = 0. \tag{31}$$

At a bifurcation point, the multiplication of Eq. (29) by $\boldsymbol{\phi}^{\mathrm{t}}$ leads to

$$\boldsymbol{\phi}^{\mathrm{t}}(\mathbf{K}_{,\mathbf{u}}\dot{\mathbf{u}}\dot{\mathbf{u}} + 2\mathbf{K}_{,\lambda}\dot{\mathbf{u}}\dot{\lambda} + \mathbf{r}_{,\lambda\lambda}\dot{\lambda}^2) = \mathbf{0}, \tag{32}$$

which after the substitution of (30) yields the algebraic bifurcation equation

$$a\xi_1^2 + 2b\xi_0\xi_1 + c\xi_0^2 = 0, \tag{33}$$

where

$$\begin{aligned} a &= \boldsymbol{\phi}^{\mathrm{t}}\mathbf{K}_{,\mathbf{u}}\boldsymbol{\phi}\boldsymbol{\phi}, \\ b &= \boldsymbol{\phi}^{\mathrm{t}}(\mathbf{K}_{,\mathbf{u}}\bar{\mathbf{u}} + \mathbf{K}_{,\lambda})\boldsymbol{\phi}, \\ c &= \boldsymbol{\phi}^{\mathrm{t}}(\mathbf{K}_{,\mathbf{u}}\bar{\mathbf{u}}\bar{\mathbf{u}} + 2\mathbf{K}_{,\lambda}\bar{\mathbf{u}} + \mathbf{r}_{,\lambda\lambda}). \end{aligned} \tag{34}$$

Defining the scalar $d = b^2 - ac$, the simple bifurcation points can be classified [28] as

$$\begin{cases} a = 0 \text{ and } b \neq 0 \Rightarrow \text{pitchfork bifurcation}, \\ a \neq 0 \text{ and } d > 0 \Rightarrow \text{transcritical bifurcation}, \\ d < 0 \Rightarrow \text{isola formation point}, \\ d = 0 \Rightarrow \text{cusp point}. \end{cases} \tag{35}$$

It is worth noting that the derivative $\mathbf{K}_{,\mathbf{u}}$, required by Eq. (34), is not generally available in a finite element program. However, approximate derivatives based on the expression

$$\mathbf{K}_{,\mathbf{u}}\mathbf{u}_1\mathbf{u}_2 = \lim_{\epsilon\to 0}\frac{\mathbf{K}(\mathbf{u}+\epsilon\mathbf{u}_1,\lambda)\mathbf{u}_2 - \mathbf{K}(\mathbf{u},\lambda)\mathbf{u}_2}{\epsilon} \tag{36}$$

can be used [29].

For sensitivity analysis purposes, the most important classification is between symmetric (pitchfork) and asymmetric bifurcations, since the computation of the sensitivity of symmetric bifurcations can be carried out using a more efficient procedure. Therefore, only the coefficient a is computed in this work and further classifications of the bifurcation points are not performed.

2.2.1. Computation of critical points

The extended system technique [30,31] can be used to accurately compute the critical points along the equilibrium path. In this work, a extended system based in the

use of Eq. (24) is applied. Thus, the system to be solved is given by

$$\begin{bmatrix} \mathbf{r}(\mathbf{u},\lambda) \\ \mathbf{K}(\mathbf{u},\lambda)\boldsymbol{\phi} \\ \|\boldsymbol{\phi}\| - 1 \end{bmatrix} = \mathbf{0}, \tag{37}$$

where the eigenvector length constraint is necessary to avoid the trivial solution ($\boldsymbol{\phi} = \mathbf{0}$). The solution of this extended system gives the critical point $(\mathbf{u},\lambda)$ as well as the buckling mode ($\boldsymbol{\phi}$), which is important not only to the critical point classification, but also to the sensitivity computation, as it will be discussed in the following sections.

The linearization of Eq. (37) yields the system

$$\begin{bmatrix} \mathbf{K} & \mathbf{0} & \mathbf{r}_{,\lambda} \\ (\mathbf{K}\boldsymbol{\phi})_{,\mathbf{u}} & \mathbf{K} & (\mathbf{K}\boldsymbol{\phi})_{,\lambda} \\ \mathbf{0}^{\mathrm{t}} & \frac{\boldsymbol{\phi}^{\mathrm{t}}}{\|\boldsymbol{\phi}\|} & 0 \end{bmatrix} \begin{bmatrix} \delta\mathbf{u} \\ \delta\boldsymbol{\phi} \\ \delta\lambda \end{bmatrix} = - \begin{bmatrix} \mathbf{r} \\ \mathbf{K}\boldsymbol{\phi} \\ \|\boldsymbol{\phi}\| - 1 \end{bmatrix}, \tag{38}$$

whose solution yields the increments $\delta\mathbf{u}$, $\delta\boldsymbol{\phi}$ and $\delta\lambda$. This system has $2N+1$ variables and equations, but it can be solved in a simple and efficient way [30], as shown in Table 1.

After the computation of the increments, the variables $(\mathbf{u},\lambda,\boldsymbol{\phi})$ are updated as indicated in Eq. (13), while the current eigenvalue (γ) can be computed from $\gamma = \boldsymbol{\phi}^{\mathrm{t}}\mathbf{K}\boldsymbol{\phi}/\boldsymbol{\phi}^{\mathrm{t}}\boldsymbol{\phi}$. The procedure stops when both the residual and the eigenvalue are smaller than prescribed tolerances.

The success in the computation of critical points using extended systems depends on the evaluation of vectors $\mathbf{h}_1$ and $\mathbf{h}_2$, which depend on the derivatives $(\mathbf{K}\boldsymbol{\phi})_{,\mathbf{u}}$ and $(\mathbf{K}\boldsymbol{\phi})_{,\lambda}$. Since the analytical computation of these derivatives is very difficult for complex elements, the finite difference method can be used to compute $\mathbf{h}_1$ and $\mathbf{h}_2$ in a simple and efficient way [31]. Using a forward difference scheme based on Eq. (36), these vectors can be computed in an element-by-element fashion by using

$$\begin{aligned} \mathbf{h}_1 &= [\mathbf{K}(\mathbf{u}+\epsilon\boldsymbol{\phi},\lambda)\delta\mathbf{u}_1 - \mathbf{K}(\mathbf{u},\lambda)\delta\mathbf{u}_1]/\epsilon + \mathbf{h}_\lambda, \\ \mathbf{h}_2 &= [\mathbf{K}(\mathbf{u}+\epsilon\boldsymbol{\phi},\lambda)\delta\mathbf{u}_2 - \mathbf{K}(\mathbf{u},\lambda)\delta\mathbf{u}_2]/\epsilon, \\ \mathbf{h}_\lambda &= [\mathbf{K}(\mathbf{u},\lambda+\Delta\lambda)\boldsymbol{\phi} - \mathbf{K}(\mathbf{u},\lambda)\boldsymbol{\phi}]/\Delta\lambda, \end{aligned} \tag{39}$$

Table 1
Solution of the extended system

1. Solve the linear systems:
   $\mathbf{K}\,\delta\mathbf{u}_1 = \bar{\mathbf{f}}$
   $\mathbf{K}\,\delta\mathbf{u}_2 = \mathbf{r}$
2. Compute the directional derivatives:
   $\mathbf{h}_1 = (\mathbf{K}\boldsymbol{\phi})_{,\mathbf{u}}\delta\mathbf{u}_1 + (\mathbf{K}\boldsymbol{\phi})_{,\lambda}$
   $\mathbf{h}_2 = (\mathbf{K}\boldsymbol{\phi})_{,\mathbf{u}}\delta\mathbf{u}_2$
3. Solve the linear systems:
   $\mathbf{K}\,\delta\boldsymbol{\phi}_1 = \mathbf{h}_1$
   $\mathbf{K}\,\delta\boldsymbol{\phi}_2 = \mathbf{h}_2$
4. Compute the increments:
   $\delta\lambda = (\boldsymbol{\phi}^{\mathrm{t}}\delta\boldsymbol{\phi}_2 - \|\boldsymbol{\phi}\|)/\boldsymbol{\phi}^{\mathrm{t}}\delta\boldsymbol{\phi}_1$
   $\delta\mathbf{u} = \delta\lambda\delta\mathbf{u}_1 - \delta\mathbf{u}_2$
   $\delta\boldsymbol{\phi} = \delta\boldsymbol{\phi}_2 - \delta\lambda\delta\boldsymbol{\phi}_1 - \boldsymbol{\phi}$

where $\Delta\lambda$ is the same perturbation used in Eq. (23). Generally, a perturbation (ϵ) in the range $10^{-3} < \epsilon\|\boldsymbol{\phi}\|/\|\mathbf{u}\| < 10^{-8}$, leads to accurate results [5]. Additional simplification can be obtained recognizing that $\mathbf{K}\,\delta\mathbf{u}_1 = \bar{\mathbf{f}}$ and $\mathbf{K}\,\delta\mathbf{u}_2 = \mathbf{r}$. Finally, it should be noted the vector $\mathbf{h}_\lambda$ computed by forward finite differences is exact (up to small round-off errors) for structures made of linear elastic materials and temperature-independent properties.

3. Design sensitivity analysis

The objective of the design sensitivity analysis is to compute the gradients (sensitivities) of the structural responses with respect to the design variables. For nonlinear static problems, these responses include displacements, stresses and nonlinear critical loads, for both limit and bifurcation points.

The simplest way to perform the sensitivity computation is the Global Finite Difference (GFD) approach. As a practical example, the forward finite difference scheme allows to easily compute the displacement sensitivities at a given load level (λ) by using

$$\frac{\mathrm{d}\mathbf{u}}{\mathrm{d}x} = \frac{\mathbf{u}(\lambda,\overline{T}+\overline{T}'\Delta x, x+\Delta x) - \mathbf{u}(\lambda,\overline{T},x)}{\Delta x}, \tag{40}$$

where Δx is a prescribed perturbation size and $\overline{T}' = \mathrm{d}\overline{T}/\mathrm{d}x$ is the sensitivity of the temperature field. The GFD accuracy depends on the perturbation size [10], but a relative perturbation ($\eta = \Delta x/x$) between 10^{-4} and 10^{-8} generally leads to good results. Moreover, this method is independent of the element formulation and is very easy to implement. The major drawback of this method is that its application requires a new nonlinear finite element analysis for each design variable, leading to a high computational cost and limiting its practical use to problems with a very small number of design variables.

The optimization of practical problems require the use of efficient methods to sensitivity computation, as the Analytical and Semi-Analytical Methods. The starting point of both methods is the system of equilibrium equations of a finite element model

$$\mathbf{g}(\mathbf{u},\lambda,\overline{T},x) - (\mathbf{f}_{\mathrm{c}}(x) + \lambda\mathbf{f}(x)) = \mathbf{0}, \tag{41}$$

where $\mathbf{u}$, λ and $\overline{T}$ are implicit functions of the design variable x. The differentiation of this equation with respect to x yields

$$\frac{\partial\mathbf{g}}{\partial\mathbf{u}}\frac{\mathrm{d}\mathbf{u}}{\mathrm{d}x} + \frac{\partial\mathbf{g}}{\partial\lambda}\frac{\mathrm{d}\lambda}{\mathrm{d}x} + \frac{\partial\mathbf{g}}{\partial\overline{T}}\frac{\mathrm{d}\overline{T}}{\mathrm{d}x} + \frac{\partial\mathbf{g}}{\partial x} - \frac{\mathrm{d}\mathbf{f}_{\mathrm{c}}}{\mathrm{d}x} - \frac{\mathrm{d}\lambda}{\mathrm{d}x}\mathbf{f} - \lambda\frac{\mathrm{d}\mathbf{f}}{\mathrm{d}x} = \mathbf{0}. \tag{42}$$

However, considering that $\mathbf{K} = \partial\mathbf{g}/\partial\mathbf{u}$ and $\bar{\mathbf{f}} = \mathbf{f} - \mathbf{g}_{,\lambda}$, this expression can be rewritten as

$$\mathbf{K}\frac{\mathrm{d}\mathbf{u}}{\mathrm{d}x} = \frac{\mathrm{d}\lambda}{\mathrm{d}x}\bar{\mathbf{f}} + \mathbf{p}, \tag{43}$$

where the so-called 'pseudo-load' vector ($\mathbf{p}$) is given by

$$\mathbf{p} = \frac{\mathrm{d}\mathbf{f}_c}{\mathrm{d}x} + \lambda\frac{\mathrm{d}\mathbf{f}}{\mathrm{d}x} - \frac{\partial \mathbf{g}}{\partial x} - \frac{\partial \mathbf{g}}{\partial \overline{T}}\frac{\mathrm{d}\overline{T}}{\mathrm{d}x}. \tag{44}$$

3.1. Regular states

In order to obtain a satisfactory design it is necessary to limit the displacements and stresses developed in the structure during the loading history. This is particularly important for certain imperfect structures that can present large displacements, but no critical states. Therefore, it is important to compute the design sensitivities of displacements and stresses at regular states along the equilibrium path.

Considering a *fixed* load level, the term $\mathrm{d}\lambda/\mathrm{d}x$ vanishes. Since the tangent stiffness matrix ($\mathbf{K}$) is nonsingular at regular points, the sensitivity of the nodal displacements can be computed from the solution of the linear system

$$\mathbf{K}\frac{\mathrm{d}\mathbf{u}}{\mathrm{d}x} = \mathbf{p}. \tag{45}$$

After the computation of the displacement sensitivities, the stress sensitivities can be easily evaluated as

$$\frac{\mathrm{d}\boldsymbol{\sigma}}{\mathrm{d}x} = \frac{\partial \boldsymbol{\sigma}}{\partial x} + \frac{\partial \boldsymbol{\sigma}}{\partial \mathbf{u}}\frac{\mathrm{d}\mathbf{u}}{\mathrm{d}x} + \frac{\partial \boldsymbol{\sigma}}{\partial \overline{T}}\frac{\mathrm{d}\overline{T}}{\mathrm{d}x}, \tag{46}$$

where

$$\frac{\partial \boldsymbol{\sigma}}{\partial \mathbf{u}} = \frac{\partial \boldsymbol{\sigma}}{\partial \boldsymbol{\varepsilon}}\frac{\partial \boldsymbol{\varepsilon}}{\partial \mathbf{u}} = \mathbf{C}\overline{\mathbf{B}}. \tag{47}$$

For uncoupled problems, term $\mathrm{d}\overline{T}/\mathrm{d}x$ vanishes and Eqs. (44)–(46) reduce to the same expressions used for sensitivity computation of nonlinear structures subjected only to mechanical loading [32,15]. Therefore, no new implementations are required to compute displacement and stress sensitivities of uncoupled problems, provided that the thermal effects are included in the stress computation through Eq. (5).

3.2. Critical states

In practical problems it is necessary to obtain a design with a required load carrying capacity. Therefore, it is important to include stability constraints and to compute the sensitivity of the critical load factor. Multiplying Eq. (43) by $\boldsymbol{\phi}^{\mathrm{t}}$ and using the critical condition ($\boldsymbol{\phi}^{\mathrm{t}}\mathbf{K} = \mathbf{0}$) it is possible to write

$$\frac{\mathrm{d}\lambda}{\mathrm{d}x} = -\frac{\boldsymbol{\phi}^{\mathrm{t}}\mathbf{p}}{\boldsymbol{\phi}^{\mathrm{t}}\bar{\mathbf{f}}}. \tag{48}$$

It should be noted that the above equation is similar to the expression previously deduced for the standard case of mechanical loading [33], but using $\bar{\mathbf{f}}$ instead of $\mathbf{f}$ and with the pseudo-load vector ($\mathbf{p}$) including the effects of the sensitivity of the temperature field ($\mathrm{d}\overline{T}/\mathrm{d}x$). It is interesting that this is the same modification required in the extension of the path-following methods to deal with thermal loading, as discussed in Section 2.1.

The computation of the critical load sensitivity using Eq. (48) is simple and efficient, once the buckling mode ($\boldsymbol{\phi}$) was already evaluated during the determination of the critical point. However, according to Eq. (28), this expression can be used only for limit points, since $\boldsymbol{\phi}^{\mathrm{t}}\bar{\mathbf{f}} = 0$ at bifurcation points.

The sensitivity computation at a bifurcation point requires the consideration of the critical condition

$$\mathbf{K}(\mathbf{u}, \lambda, \overline{T}, x)\boldsymbol{\phi}(x) = \mathbf{0}. \tag{49}$$

The differentiation of this equation w.r.t. x yields

$$\frac{\mathrm{d}(\mathbf{K}\boldsymbol{\phi})}{\mathrm{d}x} = \frac{\partial(\mathbf{K}\boldsymbol{\phi})}{\partial \mathbf{u}}\frac{\mathrm{d}\mathbf{u}}{\mathrm{d}x} + \frac{\partial(\mathbf{K}\boldsymbol{\phi})}{\partial \lambda}\frac{\mathrm{d}\lambda}{\mathrm{d}x} + \left(\frac{\partial \mathbf{K}}{\partial x} + \frac{\partial \mathbf{K}}{\partial \overline{T}}\frac{\mathrm{d}\overline{T}}{\mathrm{d}x}\right)\boldsymbol{\phi} + \mathbf{K}\frac{\partial \boldsymbol{\phi}}{\partial x} = \mathbf{0}, \tag{50}$$

which depends on the sensitivity of the nodal displacements ($\mathrm{d}\mathbf{u}/\mathrm{d}x$). Using Eq. (43), this sensitivity can be written as

$$\frac{\mathrm{d}\mathbf{u}}{\mathrm{d}x} = \frac{\mathrm{d}\lambda}{\mathrm{d}x}\delta\mathbf{u}_f + \delta\mathbf{u}_p \quad \text{with} \quad \begin{cases} \mathbf{K}\,\delta\mathbf{u}_f = \bar{\mathbf{f}}, \\ \mathbf{K}\,\delta\mathbf{u}_p = \mathbf{p}. \end{cases} \tag{51}$$

Therefore the substitution of (51) in (50) leads to

$$\frac{\mathrm{d}\lambda}{\mathrm{d}x}[(\mathbf{K}\boldsymbol{\phi})_{,\mathbf{u}}\delta\mathbf{u}_f + (\mathbf{K}\boldsymbol{\phi})_{,\lambda}] + (\mathbf{K}\boldsymbol{\phi})_{,\mathbf{u}}\delta\mathbf{u}_p + \mathbf{w} + \mathbf{K}\frac{\partial \boldsymbol{\phi}}{\partial x} = \mathbf{0}, \tag{52}$$

where

$$\mathbf{w} = \left(\frac{\partial \mathbf{K}}{\partial x} + \frac{\partial \mathbf{K}}{\partial \overline{T}}\frac{\mathrm{d}\overline{T}}{\mathrm{d}x}\right)\boldsymbol{\phi}. \tag{53}$$

Finally, the expression for computation of the sensitivity of critical loads is obtained by multiplying the above equation by $\boldsymbol{\phi}^{\mathrm{t}}$ and using the condition $\boldsymbol{\phi}^{\mathrm{t}}\mathbf{K} = \mathbf{0}$, yielding

$$\frac{\mathrm{d}\lambda}{\mathrm{d}x} = -\frac{\boldsymbol{\phi}^{\mathrm{t}}(\mathbf{h}_p + \mathbf{w})}{\boldsymbol{\phi}^{\mathrm{t}}(\mathbf{h}_f + \mathbf{h}_\lambda)}, \tag{54}$$

where

$$\begin{cases} \mathbf{h}_\lambda = (\mathbf{K}\boldsymbol{\phi})_{,\lambda}, \\ \mathbf{h}_f = (\mathbf{K}\boldsymbol{\phi})_{,\mathbf{u}}\delta\mathbf{u}_f, \\ \mathbf{h}_p = (\mathbf{K}\boldsymbol{\phi})_{,\mathbf{u}}\delta\mathbf{u}_p. \end{cases} \tag{55}$$

The directional derivatives ($\mathbf{h}_f, \mathbf{h}_p, \mathbf{h}_\lambda$) can be computed by finite differences using an expression similar to Eq. (39).

It is important to note that Eq. (54) is valid for both limit and bifurcation points. Moreover, it avoids the computation of the eigenvector sensitivity ($\partial\boldsymbol{\phi}/\partial x$) required by other expressions [5]. However, since it requires the computation of the vectors $\mathbf{w}$, $\mathbf{h}_f$, $\mathbf{h}_p$ and $\mathbf{h}_\lambda$, its computational cost is higher then the cost of Eq. (48). Thus, Eq. (54) should be used only for bifurcation points.

An alternative procedure for the computation of the sensitivity of the critical load factor at a bifurcation point can be derived by using the adjoint approach [15,16,20].

This procedure begins with the definition of a scalar equation combining both the equilibrium and critical point conditions

$$\boldsymbol{\phi}^{\mathrm{t}}\mathbf{K}\boldsymbol{\phi} - \boldsymbol{\mu}^{\mathrm{t}}(\mathbf{g} - \lambda\mathbf{f}) = 0, \tag{56}$$

where $\boldsymbol{\mu}$ is the vector of Lagrange multipliers used to enforce the equilibrium. Using the critical condition, the differentiation of this equation yields

$$\boldsymbol{\phi}^{\mathrm{t}}\left(\frac{\partial(\mathbf{K}\boldsymbol{\phi})}{\partial\mathbf{u}}\frac{\mathrm{d}\mathbf{u}}{\mathrm{d}x} + \mathbf{h}_{\lambda}\frac{\mathrm{d}\lambda}{\mathrm{d}x} + \mathbf{w} + \mathbf{K}\frac{\partial\boldsymbol{\phi}}{\partial x}\right) - \boldsymbol{\mu}^{\mathrm{t}}\left(\mathbf{K}\frac{\mathrm{d}\mathbf{u}}{\mathrm{d}x} - \frac{\mathrm{d}\lambda}{\mathrm{d}x}\bar{\mathbf{f}} - \mathbf{p}\right) = 0. \tag{57}$$

Using Eq. (55) the expression above can be rewritten as

$$\left(\boldsymbol{\phi}^{\mathrm{t}}(\mathbf{K}\boldsymbol{\phi})_{,\mathbf{u}} - \boldsymbol{\mu}^{\mathrm{t}}\mathbf{K}\right)\frac{\mathrm{d}\mathbf{u}}{\mathrm{d}x} + \left(\boldsymbol{\phi}^{\mathrm{t}}\mathbf{h}_{\lambda} + \boldsymbol{\mu}^{\mathrm{t}}\bar{\mathbf{f}}\right)\frac{\mathrm{d}\lambda}{\mathrm{d}x} + \boldsymbol{\phi}^{\mathrm{t}}\mathbf{w} + \boldsymbol{\mu}^{\mathrm{t}}\mathbf{p} = 0. \tag{58}$$

It is possible to avoid the computation of the sensitivity of the nodal displacements ($\mathrm{d}\mathbf{u}/\mathrm{d}x$) forcing the coefficient of this term to become zero. When the stiffness matrix is symmetric, this can easily be accomplished computing $\boldsymbol{\mu}$ through the solution of the linear system

$$\mathbf{K}\boldsymbol{\mu} = \mathbf{h}_{\phi} \quad \text{with } \mathbf{h}_{\phi} = (\mathbf{K}\boldsymbol{\phi})_{,\mathbf{u}}\boldsymbol{\phi}. \tag{59}$$

Finally, combining Eqs. (58) and (59) it is possible to compute the sensitivity of the critical load factor as

$$\frac{\mathrm{d}\lambda}{\mathrm{d}x} = -\frac{\boldsymbol{\phi}^{\mathrm{t}}\mathbf{w} + \boldsymbol{\mu}^{\mathrm{t}}\mathbf{p}}{\boldsymbol{\phi}^{\mathrm{t}}\mathbf{h}_{\lambda} + \boldsymbol{\mu}^{\mathrm{t}}\bar{\mathbf{f}}}. \tag{60}$$

This expression is much more efficient than Eq. (54), since it does not require the computation of the vectors $\delta\mathbf{u}_f$, $\delta\mathbf{u}_p$, $\mathbf{h}_f$ and $\mathbf{h}_p$. This advantage increases with the number of design variables, since $\boldsymbol{\mu}$ is independent of the design variable x and needs to be computed only once. It should be noted that the directional derivative $\mathbf{h}_{\phi}$ can be computed by using a expression similar to Eq. (39).

On the other hand, the multiplication of Eq. (59) by $\boldsymbol{\phi}^{\mathrm{t}}$ leads to the condition $\boldsymbol{\phi}^{\mathrm{t}}(\mathbf{K}\boldsymbol{\phi})_{,\mathbf{u}}\boldsymbol{\phi} = 0$. Therefore, according to Eq. (34) this condition implies that the stability parameter a of Eq. (34) is zero. However, since this condition holds only for symmetric (pitchfork) bifurcations, the use of Eq. (60) is not consistent for asymmetric bifurcations [15]. In the practical implementation of the present formulation the stability parameter $a = \mathbf{h}_{\phi}^{\mathrm{t}}\boldsymbol{\phi}$ is computed to classify the bifurcation point and decide which expression will be used for sensitivity computation.

It is important to note that according to Eqs. (45), (48), (54) and (60), the sensitivity computation can be performed without additional iterations even for nonlinear structures. Moreover, the linear systems that need to be solved in the evaluation of design sensitivities involves only the stiffness matrix ($\mathbf{K}$), which was already decomposed in the analysis step. Therefore, only cheap forward and back substitutions are required, rendering the sensitivity computation process highly efficient.

The expressions presented in this work show that the computation of sensitivity of the critical load factor for structures subjected to thermal loads requires basically three modifications with respect to the standard the case of mechanical loads [34,20]. The first one is the use of $\bar{\mathbf{f}}$ instead of $\mathbf{f}$ in Eqs. (48), (51) and (60), the second one is the use of $\mathbf{h}_{\lambda}$ in Eqs. (54) and (60), while the last one is related to the consideration of the terms $\partial\mathbf{g}/\partial\overline{T}$ and $\partial\mathbf{K}/\partial\overline{T}$ in Eqs. (44) and (53) which is required only for coupled problems. It is interesting to note that the first two modifications already occurred in the extension of the path-following methods and the algorithms for critical point computation to deal with thermal loading.

4. Computational implementation

The sensitivity formulation presented in the previous section can be applied to structures subjected to pure mechanical loading, pure thermal loading and combined thermo-mechanical loading. The formulation can handle perfect and imperfect structures in both regular and critical states. In addition, it can be used for size and shape variables.

However, the analytical computation of the design sensitivities requires the determination and implementation of the analytical expressions of the derivatives of $\mathbf{f}$, $\mathbf{f}_{\mathrm{c}}$, $\mathbf{g}$, $\boldsymbol{\sigma}$, and $\mathbf{K}$ with respect to the design variables. In the case of mechanical loading and shape design variables, this approach was successfully implemented for truss and continuum isoparametric elements based on the total Lagrangian approach [20], but its extension to more complex elements is a difficult and time consuming task, even for uncoupled problems. This extension is even more complex for coupled sensitivities since the computation of terms like $\partial\mathbf{g}/\partial\overline{T}$ depend on the variation of the material properties with the temperature.

In order to avoid these difficulties, the most popular alternative is the Semi-Analytical Method (SAM). This method is also based on the general expressions presented in Section 3, but uses a numerical differentiation procedure to compute the sensitivities $\mathbf{f}'$, $\mathbf{f}'_{\mathrm{c}}$, $\mathbf{g}'$, $\boldsymbol{\sigma}'$, and $\mathbf{K}'$, where the symbol $'$ denotes differentiation w.r.t. the design variable x. It should be noted that the sensitivities $\mathbf{f}'$ and $\mathbf{f}'_{\mathrm{c}}$ are the same ones used in the case of pure mechanical loads and will not be discussed here.

Using the standard forward difference scheme, the sensitivity of the internal force vector can be computed from

$$\mathbf{g}' = \frac{\partial\mathbf{g}}{\partial x} + \frac{\partial\mathbf{g}}{\partial\overline{T}}\frac{\mathrm{d}\overline{T}}{\mathrm{d}x} = \frac{\mathbf{g}(\mathbf{u},\lambda,\overline{T}+\overline{T}'\Delta x, x+\Delta x) - \mathbf{g}(\mathbf{u},\lambda,\overline{T},x)}{\Delta x}, \tag{61}$$

and the $\mathbf{w}$ vector given by Eq. (53) can be computed by using

$$\mathbf{w} = \mathbf{K}'\boldsymbol{\phi} = \frac{\mathbf{K}(\mathbf{u}, \lambda, \overline{T} + \overline{T}'\Delta x, x + \Delta x)\boldsymbol{\phi} - \mathbf{K}(\mathbf{u}, \lambda, \overline{T}, x)\boldsymbol{\phi}}{\Delta x}. \quad (62)$$

Finally, for a fixed load factor, the element stresses depend on displacements, temperature and design variable. Therefore, the sensitivity of the element stresses can be computed from

$$\boldsymbol{\sigma}' = \frac{\boldsymbol{\sigma}(\mathbf{u} + \mathbf{u}'\Delta x, \lambda, \overline{T} + \overline{T}'\Delta x, x + \Delta x) - \boldsymbol{\sigma}(\mathbf{u}, \lambda, \overline{T}, x)}{\Delta x}. \quad (63)$$

It should be noted that the expressions above are very simple and efficient, since they compute simultaneously both direct ($\partial/\partial x$) and indirect effects (due to $\mathrm{d}\overline{T}/\mathrm{d}x$) of the variation of design variable.

The Semi-Analytical Method (SAM) combines the efficiency of the Analytical Method (AM) with the simplicity and generality of the numerical differentiation. Therefore, it is widely applied in the solution of practical structural optimization problems. However, there are some problems involving shape variables where the SAM yields large errors. As these problems do not occur in the GFD, it can be concluded that these errors are caused by the numerical differentiation of the internal force vector and of the stiffness matrix, which is inherent to the semi-analytical approach [35].

In order to avoid converge problems due to large errors in the SA sensitivities, the Refined Semi-Analytical Method (RSAM) uses orthogonality relations between the element internal forces and the rigid body motions in order to improve these sensitivities. It does not lead to exact results, since the truncations errors are inherent to the numerical differentiation, but it is able to eliminate the abnormal errors occurring in structures whose displacement field is dominated by rigid body rotations. This method has been successfully applied in the sensitivity computation of linear structures [36,17], as well as of geometrically nonlinear structures including limit points [18,19] and bifurcation points [20]. One important feature of RSAM is that the orthogonality relations used to improve the sensitivities do not depend on the element formulation, but only on the element degrees of freedom. As a consequence, its formulation and implementation is not affected by the consideration of the thermal loading.

The formulation for nonlinear analysis and sensitivity computation of structures subjected to mechanical loading presented in this work was implemented in the FEMOOP program [37,38]. Using Object-Oriented Programming (OOP) concepts a class hierarchy was implemented [20,19,4] to carry-out the sensitivity computation by using the Analytical Method, the Semi-Analytical Method or the Refined Semi-Analytical Method.

The base class (*Design Sensitivity Analysis – cDSA*) is responsible for the implementation of the general expressions for sensitivity evaluation presented in Section 3. On the other hand, the computation of the sensitivities $\mathbf{f}'$, $\mathbf{f}'_c$, $\mathbf{g}'$, $\boldsymbol{\sigma}'$, and $\mathbf{w}$, which are performed at an element basis, is different for each of the presented methods. Therefore, three different sub-classes (*cAM*, *cSAM*, *cRAM*) were created to implement the computation of the element sensitivities by using the Analytical, Semi-Analytical and Refined Semi-Analytical Methods, respectively.

In the present work, this implementation was extended to include the case of thermal loading. To this end, two important modifications were made in the base class (*cDSA*). The first one was the use of $\bar{\mathbf{f}}$ instead of $\mathbf{f}$ in Eqs. (48), (51) and (60), and the second one is the use of $\mathbf{h}_\lambda$ in Eqs. (54) and (60). Moreover, to deal with coupled problems, the three sub-classes implementing the computation of the sensitivities $\mathbf{g}'$, $\boldsymbol{\sigma}'$, and $\mathbf{w}$ for each element should be modified to include the terms related to the temperature sensitivity ($\mathrm{d}\overline{T}/\mathrm{d}x$).

In order to allow the use of existing sub-classes without modification of the computer code, an alternative approach was adopted here. The first step to understand the adopted scheme is to recognize that the element sensitivities, such as $\mathbf{g}'$, can be written as the sum of two terms

$$\mathbf{g}' = \mathbf{g}'_x + \mathbf{g}'_\mathrm{T} = \frac{\partial \mathbf{g}}{\partial x} + \frac{\partial \mathbf{g}}{\partial \overline{T}}\frac{\mathrm{d}\overline{T}}{\mathrm{d}x}, \quad (64)$$

where the first one ($\mathbf{g}'_x$) represents the conventional derivatives used for the mechanical loads and the other one ($\mathbf{g}'_\mathrm{T}$) accounts for the thermal effects and should be considered only for coupled problems (i.e. $\mathrm{d}\overline{T}/\mathrm{d}x \neq 0$). The sensitivity $\mathbf{g}'_x$ is then computed using the existing implementation of Analytical, Semi-Analytical and Refined Semi-Analytical Methods. On the other hand, the sensitivity $\mathbf{g}'_\mathrm{T}$ is always computed using finite differences:

$$\mathbf{g}'_\mathrm{T} = \frac{\partial \mathbf{g}}{\partial \overline{T}}\frac{\mathrm{d}\overline{T}}{\mathrm{d}x} = \frac{\mathbf{g}(\mathbf{u}, \lambda, \overline{T} + \overline{T}'\Delta x, x) - \mathbf{g}(\mathbf{u}, \lambda, \overline{T}, x)}{\Delta x}. \quad (65)$$

Since this expression does not depend on the element type and on material parameters, it can be implemented only once in the base class and used together with the conventional sensitivities ($\mathbf{g}'_x$) computed by one of the three sub-classes discussed previously. Obviously, the same procedure can be applied to the computation of $\boldsymbol{\sigma}'$ and $\mathbf{w}$.

This approach not only avoids modifications in the code of the sub-classes, but also is fully consistent with the numerical differentiation approach applied during the nonlinear analysis to compute $\mathbf{g}_{,\lambda}$ and the directional derivatives by using Eqs. (23) and (39), respectively. Moreover, it should be recognized that Eq. (65) yields exact results for the common case of temperature-independent material properties. However, it is important to note that, in the approach applied here, the use of the Analytical Method implies that the partial derivatives with respect to the design variables are exactly computed, but that the partial derivatives depending on the temperature field are computed in an approximate way.

5. Numerical examples

In this section, a set of numerical examples including both uncoupled and coupled problems will be used to val-

idate the techniques presented in this work to the sensitivity analysis of nonlinear structures subjected to thermal loading. Perfect and imperfect structures in regular and critical states will be considered. The results obtained by the proposed formulation will be compared with sensitivities obtained from analytical closed-form solutions. For cases where closed-form solutions are not available, the sensitivities computed by the Global Finite Difference (GFD) approach will be used for comparison.

The examples include structures discretized using elements based on the total Lagragian or corotational formulations. Depending on the element type, the Analytical or the Semi-Analytical approaches will be used. The accuracy of both conventional and refined SA sensitivities for several perturbation will be studied. It is important to note that the boundary layer approach [39] for shape sensitivity analysis was not adopted in this work and the interior nodes of the finite element mesh are also perturbed in the sensitivity computation.

5.1. Two-bar truss

The first example is the two-bar truss depicted in Fig. 2. The numerical data used here are: $b = 1.0$ m, $h = 0.1$ m, $A_2/A_1 = 5$, $E = 200$ GPa, and $\alpha = 12 \times 10^{-6}/°C$, where A is the cross section area.

Considering temperature independent properties and assuming a linear elastic relation between the Green–Lagrange strains and the second Piola–Kirchhoff stresses, it can be easily shown that the temperature–displacement curve of the truss above is given by

$$\Delta T = \frac{1}{2\alpha}\left[\frac{v^2}{L_2^2} + \frac{EA_1}{EA_2}\frac{L_2}{L_1}\frac{(2h+v)(h+v)}{L_1^2}\right], \tag{66}$$

where L_1 and L_2 represents the initial lengths of the bars and v is the vertical displacement of the central node.

The temperature–displacement curve was numerically computed here using total Lagrangian elements and the Arc-Length Method. After the critical point computation the branch switching was performed and the secondary paths were traced. The complete equilibrium paths are depicted in Fig. 3. The obtained results show an asymmetric bifurcation, with one stable and other unstable secondary paths. For this simple structure, a perfect match is obtained by the numerical (FEM) results and the analytical solution given by Eq. (66).

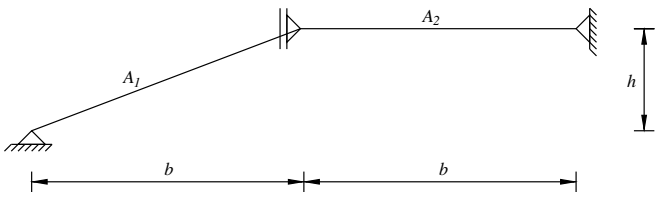

Fig. 2. Two-bar truss.

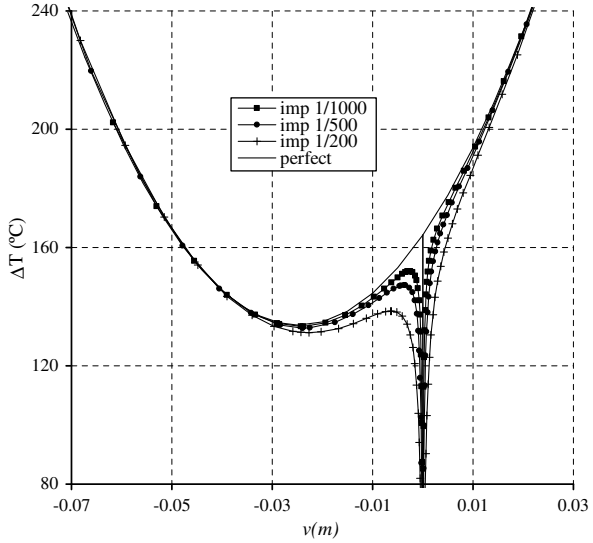

Fig. 3. Two-bar truss – equilibrium paths.

For this simple truss, a geometric imperfection can be defined as a perturbation (a) of the vertical coordinate of the central node. The results obtained for three ratios a/h are also presented in Fig. 3. These results clearly show that the geometric imperfection eliminates the bifurcation point, leading to a stable behavior for positive imperfections and an initially unstable behavior for negative imperfections.

Fig. 3 shows that the perfect truss has two critical points: one bifurcation and one limit point. The bifurcation temperature can be easily computed by setting $v = 0$ in Eq. (66), yielding

$$\Delta T_{cr} = \frac{1}{\alpha}\frac{EA_1}{EA_2}\frac{L_2 h^2}{L_1^3}. \tag{67}$$

The differentiation of this equation with respect to the height h results in

$$\Delta T'_{cr} = \Delta T_{cr}\left(\frac{2}{h} - \frac{3h}{L_1^2}\right). \tag{68}$$

For the numerical data used here $\Delta T_{cr} = 164.198$ °C and $\Delta T'_{cr} = 3235.18$ °C/m. However, it should be noted that the safe temperature increase of this truss is given by the limit point, since there are no unstable points at smaller temperatures. The displacement at the limit point can be computed by solving the equation $d\Delta T/dv = 0$, while the substitution of this displacement in Eq. (66) leads to the safe temperature (ΔT_L). The differentiation of ΔT_L with respect to the height h leads to the exact sensitivity of the limit point ($\Delta T'_L$). The final expressions are very lengthy, but can be easily obtained using a symbolic math program. For the numerical data considered here, the results are $\Delta T_L = 133.792$ °C and $\Delta T'_L = 2643.64$ °C/m.

The sensitivity of the bifurcation and limit temperatures of the finite element model with respect to the height h was computed using the methods discussed in Section 3. For

the used truss element, the Analytical Method was available, and its application to the sensitivity computation results in exactly the same numerical results presented above for both limit and bifurcation points. These results indicates that the methodology presented here for structural analysis and sensitivity computation for nonlinear structures subjected to thermal loads is correct.

In order to assess the behavior of the SA and RSA methods, the sensitivities were evaluated by using different relative perturbations ($\eta = \Delta h/h$) and the relative errors (e) were computed and plotted in Fig. 4. Here these errors are defined as

$$e = \frac{f'_{\text{approx}} - f'_{\text{exact}}}{f'_{\text{exact}}}, \tag{69}$$

where f' denotes the sensitivity of a generic function. As expected the results show that the accuracy of both methods increase when smaller perturbations are employed until the rounding errors become dominant leading to a poor accuracy for very small perturbations. It can also be noted that the RSA sensitivities are almost two orders of magnitude more accurate than the conventional SA sensitivities for a wide range of perturbations where the total error is dominated by the truncation error ($\eta > 10^{-8}$). This behavior occurs for the sensitivities of both limit and bifurcation points.

In practical problems it is necessary to deal with imperfect structures. Therefore, the sensitivities at regular ($\Delta T_L = 180\ ^\circ\text{C}$) and critical states (first limit point) with respect the imperfection a was computed by the proposed formulation and by the GFD Method ($\eta = \Delta a/a = 10^{-5}$). The obtained results are presented in Table 2. It can be noted that a very good agreement was obtained between the proposed formulation and the global finite difference approach in both regular e critical states. The behavior for the SAM and RSAM are essentially the same presented in Fig. 4 and will not be repeated here.

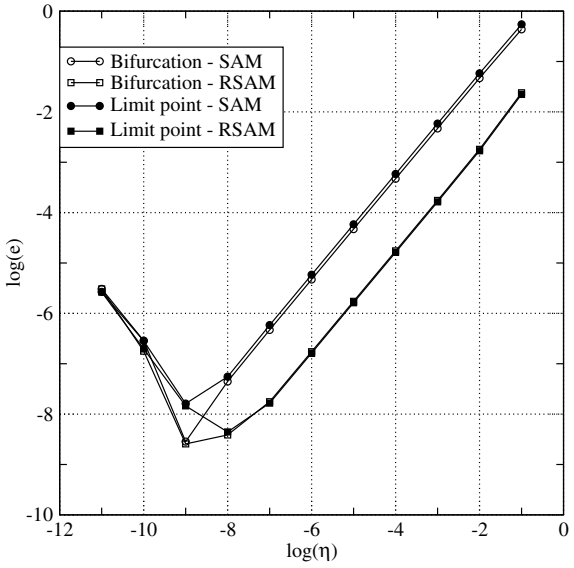

Fig. 4. Two-bar truss – sensitivity results.

Table 2
Imperfect truss – sensitivity analysis

Result	a/h	AM	GFD
$\mathrm{d}\Delta T_L/\mathrm{d}a$	−1/1000	−58244.3	−58245.9
$\mathrm{d}v/\mathrm{d}a$	1/1000	3.02062	3.02061

5.2. Slender rod

This example deals with a slender elastic rod with hinged supports and subjected to an uniform temperature rise. Fig. 5 shows the geometry and boundary conditions considered here. The axial displacement is restrained in both supports generating compressive forces and leading to thermal buckling. The following properties were used in the numerical computations: $L = 5.0$ m, $A = 10^{-3}$ m^2, $I = 2.5 \times 10^{-6}$ m^4, $E = 200$ GPa, and $\alpha = 12 \times 10^{-6}/^\circ$C, where L is the rod length and I the moment of inertia of the cross section.

The buckling temperature of this rod can be easily computed equating the compressive force generated by the temperature increase ($EA\alpha\Delta T_{\text{cr}}$) with its buckling load ($\pi^2 EI/L^2$), yielding

$$\Delta T_{\text{cr}} = \frac{\pi^2 r^2}{\alpha L^2}, \tag{70}$$

where $r = \sqrt{I/A}$ is the radius of gyration of the cross section. This equation shows that the buckling temperature does not depend on Young's modulus, but only on the thermal expansion coefficient and on the slenderness ratio (L/r). For the numerical data used here $\Delta T_{\text{cr}} = 82.2467\ ^\circ$C.

The rod was discretized using corotational plane frame elements with higher-order terms in axial strain computation [26]. Two finite element meshes (10 and 50 elements) were analyzed here using the Arc-Length Method. The critical temperatures computed here were $\Delta T_{\text{cr}} = 82.2478\ ^\circ$C for the coarse mesh and $\Delta T_{\text{cr}} = 82.2467\ ^\circ$C for the fine mesh, which are in very good agreement with the analytical results.

After the critical point computation, the secondary paths were computed and the curves of temperature versus transversal displacement of the central node (v) are presented in Fig. 6. These curves clearly show a stable-symmetric bifurcation. According to Boley and Weiner [40], the post-buckling response of this rod for moderate displacements is given by

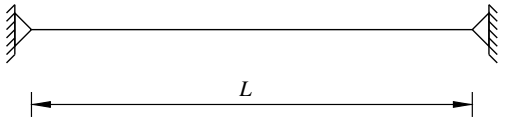

Fig. 5. Slender rod – geometry and boundary conditions.

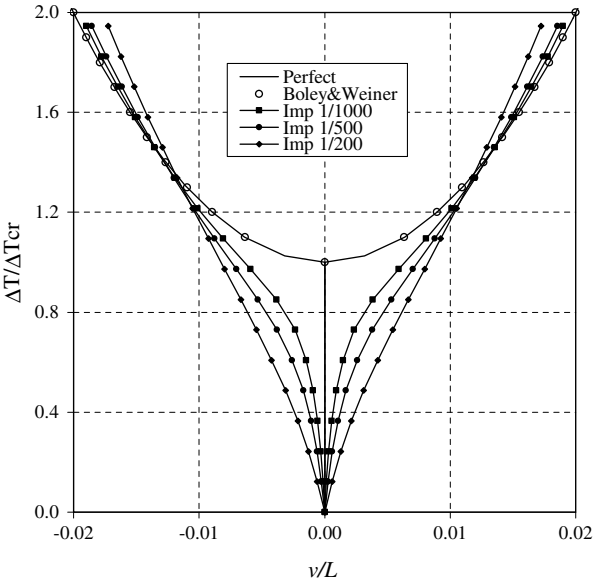

Fig. 6. Slender rod – equilibrium paths.

$$\frac{v}{L} = 2\left(\frac{r}{L}\right)\sqrt{\frac{\Delta T}{\Delta T_{\mathrm{cr}}} - 1}. \tag{71}$$

Fig. 6 shows a practically perfect agreement between the finite element solution computed here and the expected post-buckling response, validating the analysis procedure.

The buckling mode of a hinged–hinged rod has a sinusoidal shape. Thus, a half-sine wave with amplitude a was used to study the effect of geometric initial imperfections, i.e. the vertical coordinate of each nodal point. The equilibrium paths for imperfect rods with different a/L ratios are also depicted in Fig. 6. These curves present interesting features, since the initial imperfections eliminate the bifurcation point and lead initially to large displacements. However, for higher temperatures the displacements of imperfect structures are smaller than the displacements of the perfect one. Moreover, the curves for large imperfections are more linear than the curves for small imperfections. In fact, bending deformations are dominant for large imperfections, leading to a decrease in compression force due to the restrained horizontal displacement. As a consequence, the rod behavior tends to the behavior of an arch, as larger initial imperfections are considered.

The differentiation of Eqs. (70) and (71) with respect to the length (L) of the rod yields

$$\Delta T'_{\mathrm{cr}} = -\frac{2}{L}\Delta T_{\mathrm{cr}} \quad \text{and} \quad v' = \frac{4r^2}{vL}\left(\frac{\Delta T}{\Delta T_{\mathrm{cr}}}\right). \tag{72}$$

These results will be used here as reference values in the assessment of the methods for sensitivity computation discussed previously. Since the Analytical Method was not implemented for the complex nonlinear elements used in this example, only the Semi-Analytical and the Refined Semi-Analytical Methods are considered here.

In order to assess the behavior of both methods, the ratio between the FE sensitivities and the reference sensitivity computed by Eq. (72) is plotted in Fig. 7 against the relative perturbation ($\eta = \Delta L/L$). The displacement sensitivity presented in this figure was computed in the first point of the post-buckling path, where the displacements are small and the approximate response given by Eq. (71) is close to the actual response. This figure shows that both methods yield accurate results if an appropriate perturbation is adopted. However, it also shows that the Refined Semi-Analytical Method is much more reliable than the classical Semi-Analytical Method, presenting accurate results for a much wider range of perturbations. The RSA superiority is more pronounced for the fine mesh (ne = 50), where the results of the classical SA approach present large errors, specially for the sensitivity of the buckling temperature. These results show that the errors of the SA grows

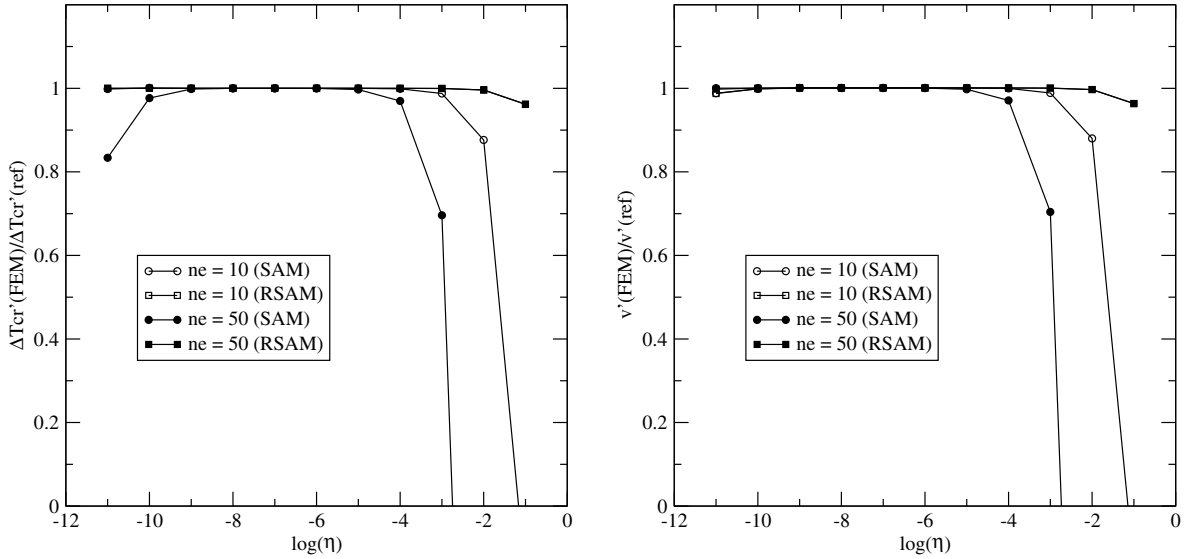

Fig. 7. Slender rod – sensitivity analysis (ne = number of elements).

with the mesh refinement and that the RSA approach eliminates this problem.

According to Fig. 6, the initial imperfections eliminate the bifurcation point generating a stable nonlinear equilibrium path. Thus, the sensitivity of the transversal displacement of the central node was computed at $\Delta T = 100\ ^\circ\text{C}$ by using $\Delta a/a = 10^{-4}$. The results obtained by using 10 corotational elements are presented in Table 3. Since exact sensitivities are not available, the GFD sensitivities can be used as reference values. It can be noted that sensitivities are in very good agreement, but that the RSAM results are much better than the SAM results.

The proposed formulation can also be applied to structures subjected to mechanical and thermal loads. Fig. 8 shows the equilibrium paths due to simultaneous action of a uniform temperature field ($T_{\text{ref}} = 0$ and $\overline{T} = 1\ ^\circ\text{C}$) and a concentrated vertical load (P) at the central node. As occurs in the case of geometric imperfections, the presence of a transverse load eliminates the bifurcation point and generates a stable nonlinear path. Therefore, the behavior in regular states due to the simultaneous action of mechanical and thermal loads should be investigated.

The sensitivity of the transversal displacement (v) of the central node was computed at $\Delta T = 100\ ^\circ\text{C}$ by using $\Delta L/L = 10^{-5}$ and 10 corotational elements. Table 4 presents the obtained results showing a very good agreement between the proposed formulation and the GFD sensitivities.

Table 3
Imperfect rod – dv/da

a/L	SAM	RSAM	GFD
1/1000	4.9108×10^{-1}	4.9316×10^{-1}	4.9315×10^{-1}
1/500	2.0399×10^{-1}	2.0561×10^{-1}	2.0560×10^{-1}
1/200	-8.7486×10^{-2}	-8.6492×10^{-2}	-8.6499×10^{-2}

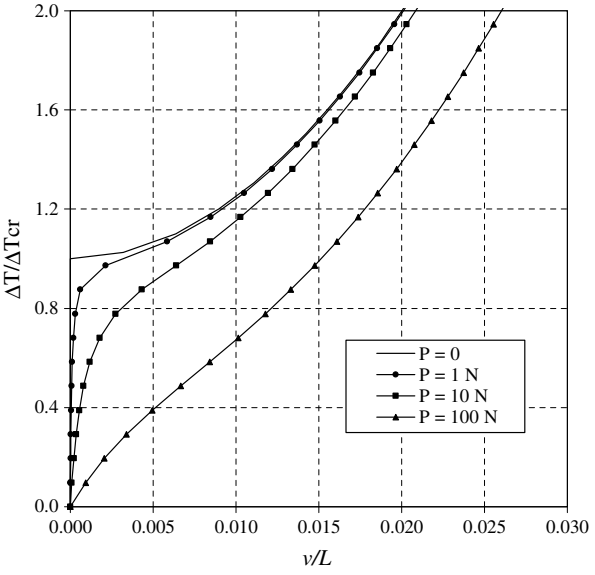

Fig. 8. Slender rod with transverse load.

Table 4
Rod with thermo-mechanical loads – dv/dL

$P(N)$	SAM	RSAM	GFD
1	5.0589×10^{-2}	5.0594×10^{-2}	5.0593×10^{-2}
10	4.2503×10^{-2}	4.2507×10^{-1}	4.2506×10^{-2}
100	3.4743×10^{-2}	3.4745×10^{-2}	3.4745×10^{-2}

5.3. Rectangular plate

A simply supported rectangular plate with constrained in-plane displacements at the boundaries and subjected to three different temperature distributions is considered here. A mesh with 12×12 quadratic quadrilateral (8-node) nonlinear plate elements based on a combination of von Karman and Mindlin theories and in a total Lagrangian formulation [26,41] was adopted for nonlinear analysis. The numerical parameters used here are: $a = 6.0$ m, $b = 6.0$ m, $t = 0.05$ m, $E = 30.6$ MPa, $\nu = 0.31$ and $\alpha = 7 \times 10^{-6}/^\circ\text{C}$, where a is horizontal length, b is the vertical length, and t is the plate thickness (Fig. 9).

In order to simplify the presentation, the plate is considered at a uniform initial temperature $T_{\text{ref}} = 0$, which leads to $\Delta T = T = \lambda \overline{T}$. The effects of three different temperature fields will be considered here. Initially, it was analyzed the effect of a uniform temperature increase $\overline{T}_1 = \overline{T}_c$. The second distribution considered here was a humped temperature profile [42] given by the equation

$$\overline{T}_2 = \overline{T}_c \sin\left(\frac{\pi x}{a}\right) \cos\left(\frac{\pi y}{b}\right). \tag{73}$$

Finally, the third case analyzed here was the temperature distribution at the steady state due to the prescribed boundary temperatures:

$$\begin{cases} \overline{T} = 0, & \text{at } y = 0, y = b, \\ \overline{T} = \overline{T}_c \sin(\pi y/b), & \text{at } x = 0, x = a. \end{cases} \tag{74}$$

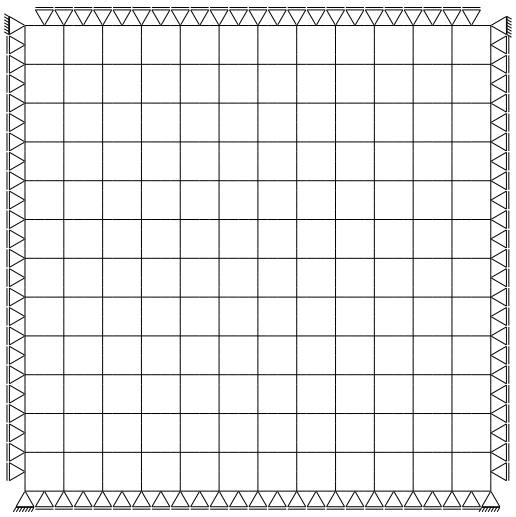

Fig. 9. Rectangular plate.

The solution of the Laplace's equation by separation of variables yields the temperature distribution for the whole plate:

$$\overline{T}_3 = \overline{T}_c\left(\frac{\sinh(\pi x/b)}{\sinh(\pi a/b)} + \cosh(\pi x/b) - \frac{\cosh(\pi a/b)}{\sinh(\pi a/b)}\sinh(\pi x/b)\right)\sin(\pi y/b). \quad (75)$$

In all the three temperature distributions it was assumed that $\overline{T}_c = 1.0$. Thus, the load factor λ represents directly the maximum temperature at a point of the plate simplifying the presentation of the computed results.

The finite element results obtained by the Arc-Length Method and an appropriate branch-switching technique [8] for each temperature distribution are plotted in Fig. 10, where v is the transversal displacement of the central node. It is important to note that the critical load factor (λ_{cr}) for each temperature distribution is quite different, but the normalized equilibrium paths are very similar. The equilibrium paths clearly show a symmetric bifurcation behavior for the three temperature distributions considered here. The symmetry of the bifurcation point can also be characterized numerically since the stability parameter a, defined by Eq. (34), is numerically equal to zero for the three temperature distributions.

In order to validate the analysis procedure, the critical load factor computed here for the first two temperature distributions were compared with the available results. For the uniform temperature distribution is easy to show that the critical temperature of a thin plate is given by

$$T_{cr} = \frac{\pi^2 t^2}{12\alpha(1+\nu)}\left(\frac{1}{a^2}+\frac{1}{b^2}\right), \quad (76)$$

which for the numerical data used here results in $T_{cr} = 12.457\,^{\circ}\mathrm{C}$. The critical temperature computed by the finite element model was 12.460 °C which represents a negligible difference with respect to the analytical value.

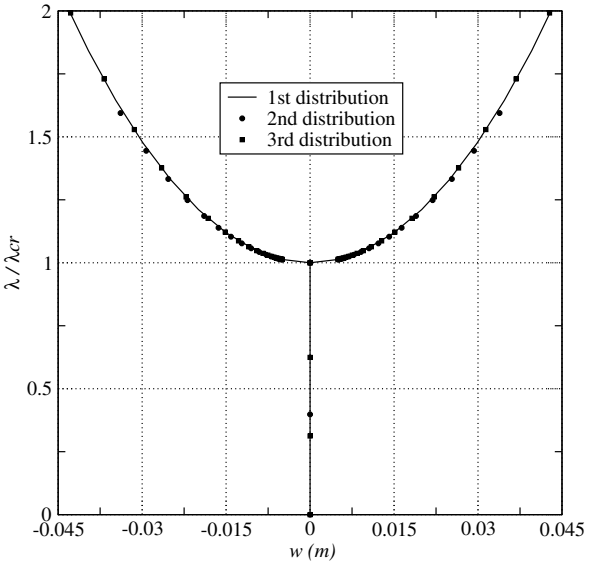

Fig. 10. Rectangular plate – equilibrium paths.

The nonuniform temperature distributions present a higher critical load factor than the uniform distribution. The ratio between critical load factors of the humped temperature profile and the uniform temperature ($\lambda_{cr}^{hump}/\lambda_{cr}^{unif}$) computed here was 1.9576, which is in very good agreement with the available reference value of 1.9721 computed by a different finite element formulation [42]. This result is important since it validates the computer implementation for nonuniform temperature fields. Finally, for the third temperature distribution the critical load factor computed here by the finite element model was $\lambda_{cr} = 32.031$.

The finite element sensitivities of the critical load factor with respect to the length a were evaluated for the three temperature distributions. It should be noted that the first two temperature distributions results in uncoupled sensitivities, since $d\overline{T}/da = 0$, while the third temperature distribution leads to coupled sensitivities ($d\overline{T}_3/da \neq 0$). In the latter case, the exact sensitivity of the temperature field was computed using a symbolic processor and used as an input data for the Analytical Method.

The finite element sensitivities computed by the Analytical Method and by the Global Finite Difference Method (with a perturbation $\Delta a = 10^{-4}$ m) are presented in Table 5. These results show that the sensitivities obtained by the two approaches are in very good agreement, indicating that the methodology presented in this work yields accurate results for both uncoupled and coupled sensitivities. It is interesting to note that the results ($\lambda'_{cr} = -4.3898$) obtained for the third distribution when the sensitivity of the temperature field is neglected is completely different from the results presented in Table 5 where this effect is included.

The sensitivities for the first temperature distribution can also be obtained by the differentiation of Eq. (76), yielding

$$T'_{cr} = \frac{dT_{cr}}{da} = -\frac{\pi^2 t^2}{6\alpha(1+\nu)a^3}. \quad (77)$$

For the numerical data used here this expression results in $T'_{cr} = -2.0762\,^{\circ}\mathrm{C/m}$. Therefore, the sensitivity computed by the proposed formulation was also in very good agreement with the theoretical value obtained by the classical plate theory (difference of only 0.24%). Finally, it is also worth noting that the numerical sensitivities computed by using Eqs. (54) and (60) approach are identical. This is an expected result since the critical point represents a symmetric bifurcation.

Table 5
Rectangular plate – λ'_{cr}

Temperature	FEM-AM	FEM-GFD
$\overline{T}_1$	−2.0712	−2.0711
$\overline{T}_2$	−4.1777	−4.1777
$\overline{T}_3$	1.6160×10^{-2}	1.6100×10^{-2}

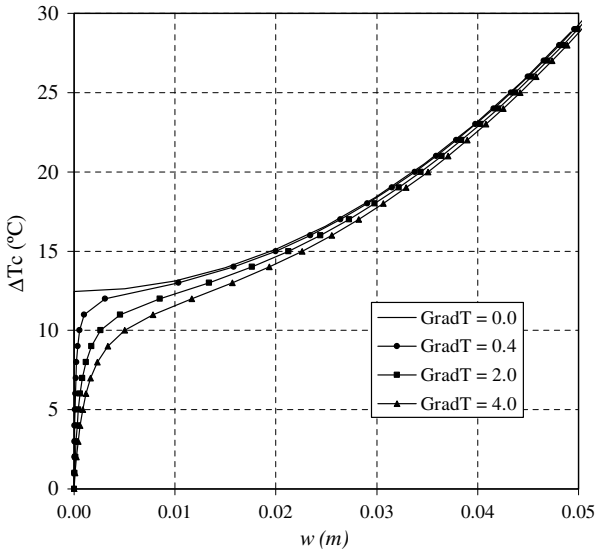

Fig. 11. Rectangular plate – $\Delta T_c = \frac{\Delta T_{top} + \Delta T_{bot}}{2}$ and GradT $= \frac{\Delta T_{top} - \Delta T_{bot}}{t}$.

Table 6
Rectangular plate – dw/da

GradT	FEM-AM	FEM-GFD
0.4	9.2798×10^{-3}	9.2794×10^{-3}
2.0	8.3921×10^{-3}	8.3918×10^{-3}
4.0	7.6942×10^{-3}	7.6940×10^{-3}

In practical applications, the temperature field may be nonuniform across the plate thickness generating bending deflections. Thus, the plate was also analyzed here considering different temperatures in top (ΔT_{top}) and bottom (ΔT_{bot}) surfaces. The computed results are presented in Fig. 11, where the curves show that the thermal gradient in the plate thickness has an effect similar to a small geometric imperfection, eliminating the bifurcation point and generating a stable equilibrium path.

Therefore, in the practical optimization of plates it is also necessary to compute sensitivities in regular states. In order to validate the proposed formulation, the sensitivity of the central deflection (w) with respect to the length a was computed by using the Analytical Method and GFD Method ($\Delta a = 10^{-4}$).

The obtained results for $\Delta T_c = 15$ °C are presented in Table 6. It can be noted that analytical and global finite-difference sensitivities are in very good agreement, validating the proposed methodology for sensitivity computation.

6. Concluding remarks

This work presented a finite element methodology for the sensitivity analysis of nonlinear structures subjected to thermal and mechanical loading. This methodology is based on the use of the effective strain concept for the structural analysis. This approach allows the consideration of thermal effects in a finite element program developed to deal with pure mechanical loading with only minor changes in the code. As a matter of fact, the use of the Load Control Method to trace the equilibrium path requires only the use of the effective strains instead of the total strains in the stress computation.

More advanced path-following methods necessary to deal with limit points (e.g. Arc-Length Method) require the computation of the derivative ($\mathbf{g}_{,\lambda}$) and the critical point computation by using extended systems require the derivative ($(\mathbf{K}\boldsymbol{\phi})_{,\lambda}$). These vectors are not required in the case of pure mechanical loading. Since the exact computation of these vectors is complex, both were successfully computed here by finite differences. The same approach is adopted for the directional derivatives of the stiffness matrix.

The expressions required for sensitivity computation of displacements, stresses, and critical loads were obtained in this work using the direct differentiation approach. The general expressions for shape and size variables were obtained for both coupled and uncoupled sensitivities. The adjoint approach was also applied for the sensitivity of the critical load factor resulting in a more efficient scheme for sensitivity computation. Unfortunately, this procedure is limited to symmetric bifurcations.

It was demonstrated that the modifications required in the expressions to compute the uncoupled sensitivities are closely related to the modifications performed in the structural analysis procedures to deal with thermal loads. On the other hand, the case of coupled sensitivities is more complex and the additional derivatives required in this case were computed here by numerical differentiation. This approach allows to deal with materials presenting temperature-dependent properties.

The proposed methodology for sensitivity analysis of nonlinear structures subjected to thermal and mechanical loading was successfully implemented in an object-oriented finite element code. The formulation and implementation of this methodology was validated by a set of numerical examples involving both perfect and imperfect structures in regular and critical states. These examples include uniform and variable temperature fields as well as coupled and uncoupled sensitivities.

A very good agreement was obtained between the FE-based analytical sensitivities computed here and the available reference values. In the case of complex finite elements, the analytical sensitivities are difficult to obtain and the classical or refined semi-analytical approaches need to be employed. The numerical examples presented here showed once again that the Refined Semi-Analytical Method is much more accurate and reliable than the classical semi-analytical approach. Therefore, this method is recommended for practical shape optimization.

Acknowledgment

The first author acknowledges CNPq for the financial support in the development of this work.

References

[1] Chen B, Gu Y, Zhao G, Lin W, Chang TYP, Kuang JS. Design optimization for structural thermal buckling. J Therm Stresses 2003;26(5):479–94.

[2] Thompson JMT, Hunt GW. A general theory of elastic instability. John Wiley and Sons; 1973.

[3] Lee S, Hinton E. Dangers inherited in shells optimized with linear assumptions. Comput Struct 2000;78:473–86.

[4] Parente Jr E. Sensitivity analysis and shape optimization of geometrically nonlinear structures, Ph.D. Thesis, Civil Engineering Department/PUC-Rio; 2000 [in Portuguese].

[5] Reitinger R, Bletzinger K-U, Ramm E. Shape optimization of buckling sensitive structures. Comput Syst Eng 1994;5(1):65–75.

[6] Mróz Z, Piekarski J. Sensitivity analysis and optimal design of nonlinear structures. Int J Numer Methods Eng 1998;42:1231–62.

[7] Bazant ZP, Cedolin L. Stability of structures – elastic, inelastic, fracture and damage theories. Oxford University Press; 1991.

[8] Parente Jr E, Holanda AS, Silva SMBA. Tracing nonlinear equilibrium paths of structures subjected to thermal loading. Comput Mech 2006;38(6):505–20.

[9] Arora J. Introduction to optimum design. McGraw Hill; 1989.

[10] Haftka RT, Gürdal Z. Elements of structural optimization. Kluwer Academic Publishers; 1992.

[11] Araujo A, Soares CMM, Herskovits J, Pedersen P. Development of a finite element model for the identification of mechanical and piezoelectric properties through gradient optimisation and experimental vibration data. Compos Struct 2002;58:307–18.

[12] Haukaas T, Scott MH. Shape sensitivities in the reliability analysis of nonlinear frame structures. Comput Struct 2006;84:964–77.

[13] Haftka RT. Techniques for thermal sensitivity analysis. Int J Numer Methods Eng 1981;17:71–80.

[14] Haftka RT, Malkus DS. Calculation of sensitivity derivatives in thermal problems by finite differences. Int J Numer Methods Eng 1981;17:1811–21.

[15] Mróz Z, Haftka RT. Design sensitivity analysis of non-linear structures in regular and critical states. Int J Solids Struct 1994;31(15):2071–98.

[16] Kleiber M. Parameter sensitivity in nonlinear mechanics. John Wiley and Sons; 1997.

[17] van Keulen F, de Boer H. Rigorous improvement of semi-analytical design sensitivities by exact differentiation of rigid body motions. Int J Numer Methods Eng 1998;42:71–91.

[18] de Boer H, van Keulen F. Refined semi-analytical design sensitivities. Int J Solids Struct 2000;37(46–47):6961–80.

[19] Parente Jr E, Vaz LE. Improvement of semi-analytical design sensitivities of non-linear structures using equilibrium relations. Int J Numer Methods Eng 2001;50(9):2127–42.

[20] Parente Jr E, Vaz LE. On the evaluation of shape sensitivities of nonlinear critical loads. Int J Numer Methods Eng 2003;56:809–46.

[21] Cook RD, Malkus DS, Plesha ME. Concepts and applications of finite element analysis. third ed. John Wiley and Sons; 1989.

[22] Bathe KJ. Finite element procedures. Prentice Hall; 1996.

[23] Batoz JL, Dhatt G. Incremental displacement algorithms for nonlinear problems. Int J Numer Methods Eng 1979;14:1262–6.

[24] Ramm E. Strategies for tracing the nonlinear response near limit points. In: Wunderlichi W, Stein E, Bathe KJ, editors. Nonlinear finite element analysis in structural mechanics. Springer-Verlag; 1981. p. 63–89.

[25] Crisfield MA. A fast incremental/iterative solution procedure that handles snap-through. Comput Struct 1981;13:55–62.

[26] Crisfield MA. Non-linear finite element analysis of solids and structures, vol. 1. John Wiley and Sons; 1991.

[27] Decker DW, Keller HB. Path following near bifurcation. Commun Pure Appl Math 1981;34(46–47):149–75.

[28] Jepson A, Spence A. Folds in the solution of two-parameter systems and their calculation, Part I. SIAM J Numer Anal 1985;22:347–68.

[29] Moore G, Spence A. The calculation of turning points of nonlinear equations. SIAM J Numer Anal 1980;17(4):567–76.

[30] Wriggers P, Wagner W, Miehe C. A quadratically convergent procedure for the calculation of stability points in finite element analysis. Comput Methods Appl Mech Eng 1988;70:329–47.

[31] Wriggers P, Simo JC. A general procedure for the direct computation of turning and bifurcation points. Int J Numer Methods Eng 1990;30:155–76.

[32] Ryu YS, Haririan M, Wu CC, Arora JS. Structural design sensitivity analysis of nonlinear response. Comput Struct 1985;21(12):245–55.

[33] Wu CC, Arora JS. Design sensitivity analysis of non-linear buckling load. Comput Mech 1988;3:129–40.

[34] Reitinger R, Ramm E. Buckling and imperfection sensitivity in the optimization of shell structures. Thin-Walled Struct 1995;23:159–77.

[35] Olhoff N, Rasmussen J, Lund E. A method of "exact" numerical differentiation for error elimination in finite-element-based semi-analytical shape sensitivity analysis. Mech Struct Mach 1993;25(8):1118–25.

[36] de Boer H, van Keulen F. Error analysis of refined semi-analytical design sensitivities. Struct Optim 1997;14:242–7.

[37] Martha LFCR, Parente Jr E. An object-oriented framework for finite element element programming. In: Proceedings of fifth World congress on computational mechanics (WCCM V), Vienna, cD-ROM; 2002. p. 1–10.

[38] Martha LFCR, Menezes IFM, Lages EN, Parente Jr E, Pitangueira RLS. An OOP class organization for materially nonlinear FE analysis. In: Proceedings of the XVII CILAMCE, Venice; 1996. p. 229–32.

[39] Olhoff N, Lund E. Finite element based engineering design sensitivity analysis and optimization. In: Herskovits J, editor. Advances in structural optimization. Kluwer Academic Publishers; 1995. p. 1–45.

[40] Boley BA, Weiner JH. Theory of thermal stresses. Dover Publications; 1997.

[41] Holanda AS. Analysis of the equilibrium and stability of plates with contact constraints, Ph.D. Thesis, Civil Engineering Department/PUC-Rio; 2000 [in Portuguese].

[42] Ko WL. Thermal buckling analysis of rectangular panels subjected to humped temperature profile heating, Technical Publication NASA/TP-2004-212041, NASA Dryden Flight Research Center; 2004.